Engineering Structures 322 (2025) 119054

Contents lists available at ScienceDirect

Engineering Structures

journal homepage: www.elsevier.com/locate/engstruct

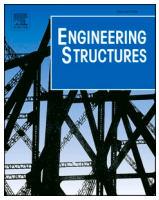

Rapid crack-based assessment of deep beams based on a single crack measurement

Boyan Mihaylov [a,*], Eissa Fathalla [a,b], Alexandru Trandafir [c]

[a] Department of ArGEnCo, University of Liège, Building B52, Quartier Polytech 1, Allée de la Découverte 9, B-4000 Liège, Belgium
[b] Structural Engineering Department, Cairo University, Giza 12613, Egypt
[c] Technical University of Civil Engineering Bucharest, Lacul Tei Bvd. 124, Bucharest, 020396, Romania

ARTICLE INFO

Keywords:
Crack-based assessment
Deep beams
Residual shear capacity
Structural monitoring

ABSTRACT

Deep beams in concrete infrastructure often exhibit wide diagonal shear cracks that extend from the supports to concentrated loads. A key problem in these cases is to assess the residual capacity against shear failure across such cracks. This problem can be solved by establishing a relationship between the opening of the crack and the residual capacity, expressed in percentage of the shear strength. The current study establishes such a relationship that requires minimal input information. The input consists of only three on-site measurements: the depth of the critical loading zone (CLZ) determined by the diagonal crack; the angle of the crack in the CLZ; and a single crack measurement: the vertical crack displacement in the vicinity of the CLZ. The physical basis of the proposed crack-based assessment (CBA) is established with the help of a targeted test and advanced modelling. It is shown that only three input parameters and two simple closed-form equations are sufficient to accurately evaluate the residual capacity of diagonally cracked deep beams with various properties. Furthermore, in the presence of loading and unloading cycles, the proposed CBA reveals how close the member has come to shear failure throughout its entire service life. These properties render the CBA not only suitable for rapid assessment, but also for long-term monitoring of deep beams with diagonal cracks.

1. Introduction

Deep reinforced concrete beams work with high shear stresses and can develop diagonal shear cracks under service loads. As shown in Fig. 1, in cantilever regions of deep beams, these major cracks extend from the inner edge of loading elements to the vicinity of support members [1]. In simply supported deep beams, the cracks extend from the supports to the vicinity of concentrated loads. Such situations arise in various important members, such as deep pier cap beams in bridges (Fig. 1) and deep transfer girders in buildings. In existing bridges, the amount of shear reinforcement often does not meet modern design requirements for crack control, thus exacerbating the opening of diagonal cracks. In recent years, crack widths of up to 0.9 mm have been reported in road bridges in operation [1–4]. This has raised serious concerns about the safety of traffic on these structures, as well as questions about the long-term monitoring of deep pier cap beams.

The behavior of deep beams has been studied both experimentally and analytically since the 1950s. Tests have shown that deep beams typically fail in shear along critical diagonal cracks with yielding of the transverse reinforcement and crushing of the concrete [5–7]. However, until recently, no studies included detailed measurements of crack displacements (i.e., crack widths and slips) and information on how they relate to the residual shear capacity of deep members. The same applies to most available modelling approaches: the focus has been predominantly on predicting the shear strength of deep beams without explicit consideration of crack displacements. The most common modelling approaches include strut-and-tie [8,9] and stress field models [10], both based on the lower-bound theorem of the theory of plasticity. However, in recent years, the use of digital image correlation (DIC) in experimental studies has allowed to measure accurately crack displacements and concrete strains [11–14]. Field measurements have also advanced with the development of computer vision and other approaches [15,16]. In this context, a key question persists: can measured cracks be used to evaluate the residual shear capacity of deep beams, as well as to monitor the safety of such members in existing structures?

In principle, this question can be formalized as illustrated with the plot in Fig. 2 [17,18]. On the horizontal axis of the plot is a crack displacement (e.g., crack width at a particular location), and on the vertical axis is the residual shear strength of the member $1\text{-}V/V_u$ in % (V

* Corresponding author.
E-mail address: boyan.mihaylov@uliege.be (B. Mihaylov).

https://doi.org/10.1016/j.engstruct.2024.119054
Received 6 June 2024; Received in revised form 30 August 2024; Accepted 26 September 2024
Available online 1 October 2024

Nomenclature

a	shear span
b	beam width (rectangular section)
a_g	maximum size of coarse aggregate
d	effective depth of section
d_{CLZ}	depth of critical section of the CLZ
E_c	modulus of elasticity of concrete
E_s	modulus of elasticity of reinforcement
f_c	concrete cylinder strength
f_y	yield strength of reinforcement
h	total depth of section
l_{b1e}	effective length of loading plate
l_t	cracked length along flexural-tensile reinforcement
T	tensile force in flexural-tensile reinforcement
P	point load
P_u	point load at failure
V	shear force
V_{CLZ}	shear resisted by the CLZ
V_{ci}	shear resisted by aggregate interlock
V_d	shear resisted by dowel action
V_s	shear resisted by stirrups
V_{res}	residual shear capacity
V_u	shear strength (shear capacity, peak resistance)
w	crack width
w_v	vertical crack displacement
$w_{v,cr}$	critical vertical crack displacement
s	crack slip
z	lever arm of internal longitudinal forces at section with maximum moment
α_{CLZ}	angle of critical diagonal crack in the CLZ
Δ	mid-span deflection
Δ_c	shear distortion of the CLZ
Δ_{cu}	displacement capacity of the CLZ
ε	compressive strains in the CLZ
ε_2	principal compressive strains
$\varepsilon_{2,max}$	maximum principal compressive strain
ε_c	strain of concrete at peak compressive stress f_c
ε_{max}	maximum compressive strain in the CLZ
$\varepsilon_{t,avg}$	average strain along flexural-tensile reinforcement
ε_v	stirrup strain
ρ_l	ratio of flexural reinforcement
ρ_v	stirrup ratio
σ	compressive stresses in the CLZ
σ_{avg}	average compressive stress in the CLZ
ψ	residual shear capacity (in %)

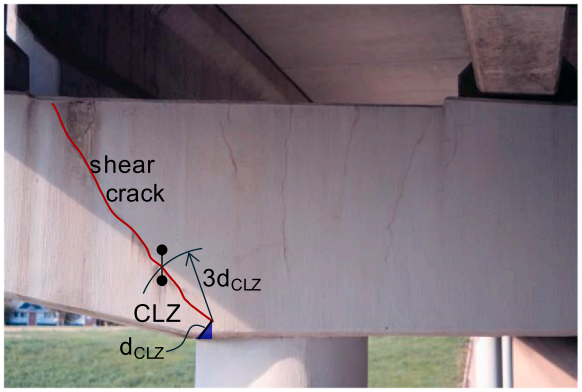

Fig. 1. Deep pier cap beam with a major diagonal shear crack (adapted from Bracci et al., 2000 [1]).

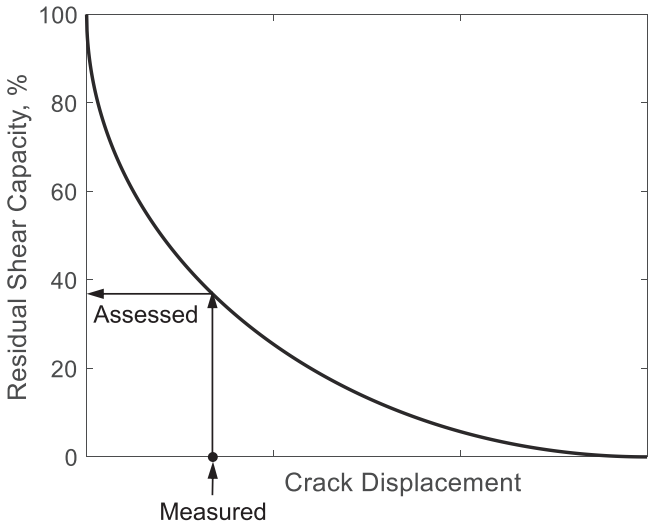

Fig. 2. Residual shear capacity diagram for direct crack-based assessment.

is the shear force and V_u the shear resistance). The residual capacity decreases with the opening of the crack and reaches zero when the beam is at peak load (shear failure). If such residual capacity diagrams are prepared in advance, they can be used for direct crack-based assessment (CBA) as illustrated with the arrows in Fig. 2. For a measured crack displacement, the diagram allows to rapidly evaluate the residual shear capacity of the member and inform appropriate measures.

To generate residual capacity curves for deep beams, Trandafir et al. [17,18] have proposed a crack-based assessment method (CBA) using the Two-Parameter Kinematic Theory (2PKT) [19,20]. In this method, the crack geometry is measured and used as an input for 2PKT simulations, together with the geometrical and material properties of the member. In this manner, it has been shown that the method captures the influence the crack shape can have on the shear resistance. In limit cases, a strength difference of up to 60 % has been observed and predicted between nominally identical beams whose crack shapes differed due to random factors. More recently, a crack-based assessment method has been proposed by Fathalla and Mihaylov [13] for short (non-slender) shear walls with diagonal cracks. The method focuses on evaluating the state of damage in the compression toe of the wall based solely on crack measurements. More precisely, it evaluates the displacement capacity of these critical zones and compares it to the measured displacement sustained by the zone. Earlier research on crack-based assessment includes methods for panels by Calvi et al. [21] and slender (non-deep) beams by Zaborac et al. [22], both largely based on the Modified Compression Field Theory [23].

The goal of this paper is to demonstrate that residual capacity diagrams for deep beams can be obtained with an extremely parsimonious yet accurate approach, requiring minimal input and computational effort. It will be shown that only two simple closed-form equations are completely sufficient to accurately capture the response shown in Fig. 2 for beams with various properties (e.g., aspect ratio, amount of reinforcement, material properties). The only inputs to the equations are three measurements performed on the cracked member: a distance, a crack angle, and a crack displacement. Detailed experimental observations and the CBA method proposed by Trandafir et al. [17,18] are used

to establish the physical basis of the proposed equations. The paper also addresses the important question concerning the effect of loading history in the context of crack-based assessment of deep members subjected to loading and unloading. The novelty of the proposed approach for deep beams lies in the combination of physical basis, simplicity, accuracy, and explaining power.

2. Experimental observations

2.1. Description of test P8

To answer important questions about crack-based assessment, a targeted test of a full-scale deep beam was conducted in this study. The key features of the test were a targeted instrumentation and a loading history involving cycles of unloading and reloading.

Fig. 3 shows the geometrical and material properties of the beam, named specimen P8. The shear-span-to-effective-depth ratio of the specimen was a/d= 1.64, the flexural reinforcement ratio was ρ_l= 1.37 %, and the transverse reinforcement ratio was ρ_v= 0.134 %. The beam was subjected to symmetrical three-point bending through 180-mm-long loading and support steel plates. On one face of the beam, a zone of 600 mm by 350 mm in the vicinity of the loading plate was speckled for high-resolution digital image correlation (DIC) measurements (Fig. 3). On the opposite face of the beam, displacement transducers were used to measure the deflection of the specimen and various deformations on the concrete surface.

2.2. Observed behavior of specimen P8

The complete shear force versus deflection response of specimen P8 is shown in Fig. 4. The crack pattern at failure and measured crack widths at different load stages are reported in Fig. 5. The load was applied in three major load cycles with increasing peak shear forces: 300 kN, 375 kN and 450 kN (points 1, 2 and 3 in Fig. 4). In all cycles the unloading was performed to 200 kN to simulate permanent (dead) load on structures (points 1′, 2′ and 3′ in Fig. 4). The average loading rate was 2 kN/sec. Manual crack measurements were performed at the load levels marked on the V-Δ curve after 10 % uploading each time.

After an initial linear-elastic response, flexural and flexure-shear cracks developed in the two shear spans. The major diagonal cracks formed at a shear force of approximately 225 kN, or 49 % of the peak resistance (shear strength). They extended from the inner edges of the supports to the vicinity of the load, and reached widths of up to 1.8 mm at 88 % of V_u prior to failure (Fig. 5). The failure occurred at V_u= 459 kN with sudden widening of the east (E) diagonal crack and crushing of the concrete in the vicinity of the load. More precisely, the crushing

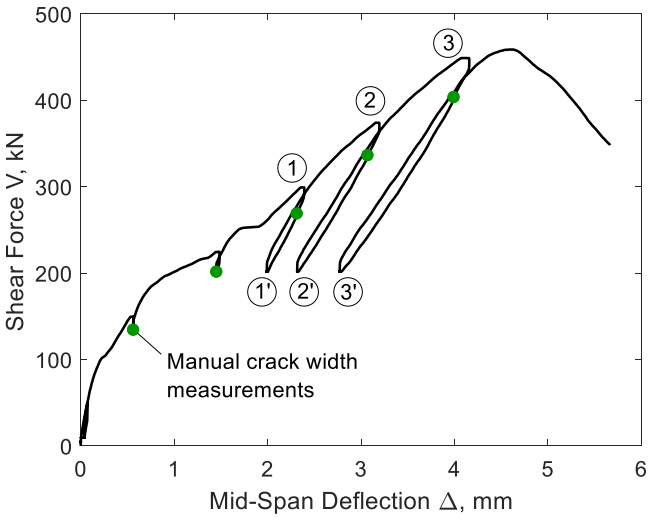

Fig. 4. Global response of specimen P8.

occurred above the critical crack near the edge of the loading plate. This zone of high damage has been referred to as the critical loading zone (CLZ) [19] as it typically triggers the failure of deep beams. For this reason, the CLZ will be key for developing a parsimonious crack-based assessment approach later in this study.

The deformations in the CLZ of specimen P8 are studied in more detail with the help of the DIC measurements. Fig. 6a shows the deformed configuration of the CLZ (scaled ×30) at the three pairs of maximum and minimum levels of loading and unloading, respectively. The loading reached 65.4 %, 81.7 % and 98.1 % of the peak load (points 1, 2 and 3 in Fig. 4), while the unloading was always performed to 44 % of V_u (points 1′, 2′ and 3′ in Fig. 4). The diagrams show clear shear distortions of the critical loading zone, particularly at 98.1 % of V_u when inclined macrocracks formed in the CLZ due to high diagonal compressive stresses. The shear deformations result in nearly vertical displacements in the critical crack in the vicinity of the load. This is illustrated with the vector in the deformed shape at 98.1 % of V_u, which has a relatively very small horizontal component. Because the crack displacement is nearly vertical and the crack is inclined, the critical diagonal crack undergoes a combination of crack opening and crack slip.

The DIC data allows to measure the vertical displacements in the critical crack by installing virtual displacement transducers. One such transducer is marked in Fig. 6a at a horizontal distance of 183 mm from the center of the load in the critical east shear span (see point A along the crack). The choice of this particular distance/point is intentional and

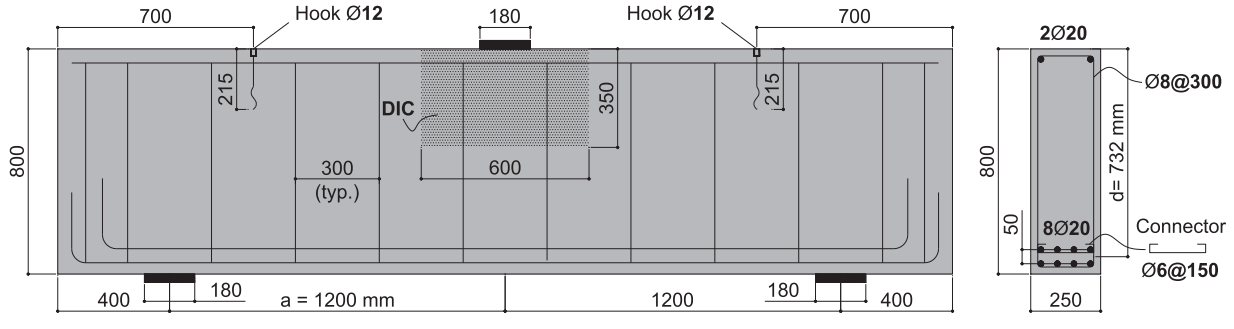

Concrete Properties

f_c=39.7 MPa
E_c=25.8 GPa
ε_c= 2.4×10^{-3} at f_c

Reinforcement Properties

Ø20
f_y=534 MPa, f_u=616 MPa
E_s=203 GPa, ε_u=97 ×10^{-3}

Ø8
f_y=523 MPa, f_u=595 MPa
E_s=174 GPa, ε_u=50×10^{-3}

Fig. 3. Beam geometry, reinforcement, and material properties of specimen P8.

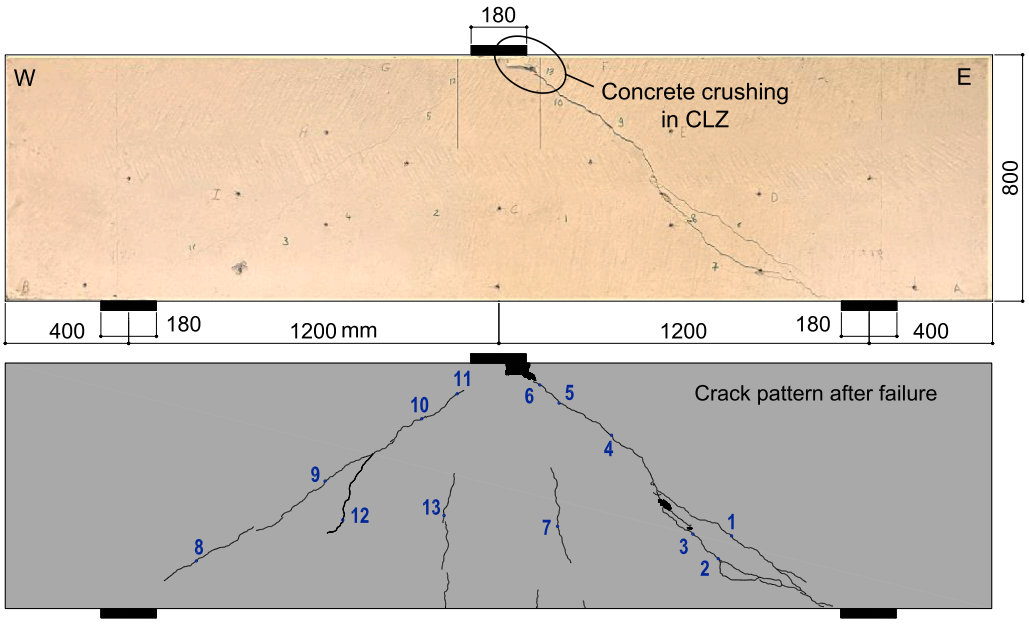

V/V$_u$	Crack Width (mm) at Point												
(%)	1	2	3	4	5	6	7	8	9	10	11	12	13
29	-	-	-	-	-	-	0.17	-	-	-	-	-	0.14
44	0.17	0.25	0.43	0.34	0.18	-	0.20	0.14	0.25	0.19	-	0.23	0.16
59	0.39	0.34	0.67	0.55	0.33	0.08	0.23	0.33	0.40	0.44	0.07	0.37	0.18
74	0.70	0.61	0.99	0.95	0.66	0.24	0.28	0.65	0.70	0.62	0.19	0.41	0.20
88	1.17	0.89	1.12	1.76	1.11	0.63	0.30	0.75	1.17	0.84	0.28	0.42	0.22

Fig. 5. Photograph and crack pattern at failure of specimen P8.

will be discussed in detail in Section 3.2. The measurement of the transducer is denoted $w_{v,cr}$ – the critical vertical crack displacement. This displacement is aimed to characterize the deformations and damage in the critical loading zone. The transducer spans the critical crack and extends to the top edge of the beam. In this way, prior to the formation of cracks inside the CLZ, the transducer measured the vertical displacement in the critical crack. After the cracking in the CLZ occurred at 97 % of V_u, the transducer also captured the rapid vertical expansion of the CLZ. It can be seen that as the shear was increased from 65.4 % to 98.1 % of V_u, $w_{v,cr}$ increased significantly from 0.23 mm to 0.84 mm (3.65 times). In a sharp contrast, upon unloading, the critical vertical crack displacement $w_{v,cr}$ changed only slightly (see pairs 1–1′, 2–2′, 3–3′). For instance, when the beam was unloaded from 98.1 % to 44 % of V_u, $w_{v,cr}$ recovered by only 5 %. In other words, the unloading behavior in terms of V versus $w_{v,cr}$ is almost perfectly plastic (vertical branch). This vertical unloading is a very important property of the critical vertical crack displacement, which will be exploited further in this study for the purpose of meaningful crack-based assessment and monitoring.

The state of the CLZ at failure of specimen P8 is shown in Fig. 6b. In addition to the deformed shape, the figure also shows a color map of the principal compressive strains ε_2 and a photograph of the crushed CLZ after the test. The inclined cracking in the concrete was extensive and the critical vertical crack displacement $w_{v,cr}$ reached 1.40 mm. This is an increase of 0.56 mm compared to the measured value at 98.1 % of the failure load. The compressive strains in the CLZ exceeded 3×10^{-3} and were oriented largely parallel to the critical diagonal crack. This is consistent with the observed crushing of the concrete and the orientation of the inclined cracks in the CLZ. Higher strains were observed near the bottom of the CLZ as illustrated with the white diagram within the color map. This diagram shows the strain variation across a section which is perpendicular to the critical crack. An approximation of these strains at failure will be used later for the purpose of crack-based assessment.

3. 2PKT analysis of test P8

3.1. Brief overview of crack-based 2PKT

To gain further understanding of specimen P8, its behavior is modelled using the advance crack-based assessment approach (CBA) proposed by Trandafir et al. [17,18] based on the Two-Parameter Kinematic Theory (2PKT) [19,20]. As this approach has been formulated and discussed in detail elsewhere [17,18], it is only summarized here before discussing its predictions for beam P8.

Fig. 7 illustrates the main steps and components of the CBA. This approach is applicable to shear-critical deep beams, which have developed complete diagonal cracks between the loading and support points. As shown in Fig. 7 (top), the assessment of such members consists of two main steps. First, the geometry of the potential critical diagonal crack is measured onsite and represented as a series of short straight segments. To achieve detailed modelling of aggregate interlock across the crack, the length of the segments is selected approximately equal to the maximum size of the coarse aggregates a_g. Second, the measured crack geometry, together with the main properties of the beam (i.e., dimensions, reinforcement and material properties), is used as an input to the Two-Parameter Kinematic Theory. The 2PKT is in turn used to simulate the complete shear response of the beam up to failure, taking into account the specific geometry of the measured crack. The 2PKT is well suited for such simulations as it explicitly models the kinematics of the critical cracks based on a kinematic model with two degrees of freedom (DOFs).

Fig. 7a-c summarise the 2PKT, which consists of three components: a) kinematics (compatibility of deformations), b) constitutive relationships for the shear-resisting mechanisms, and c) equilibrium. As shown in Fig. 7a, the two DOFs of the 2PKT are associated with two distinct deformation patterns, which are superimposed to model the complete deformed shape of the beam. The first DOF is the average strain along

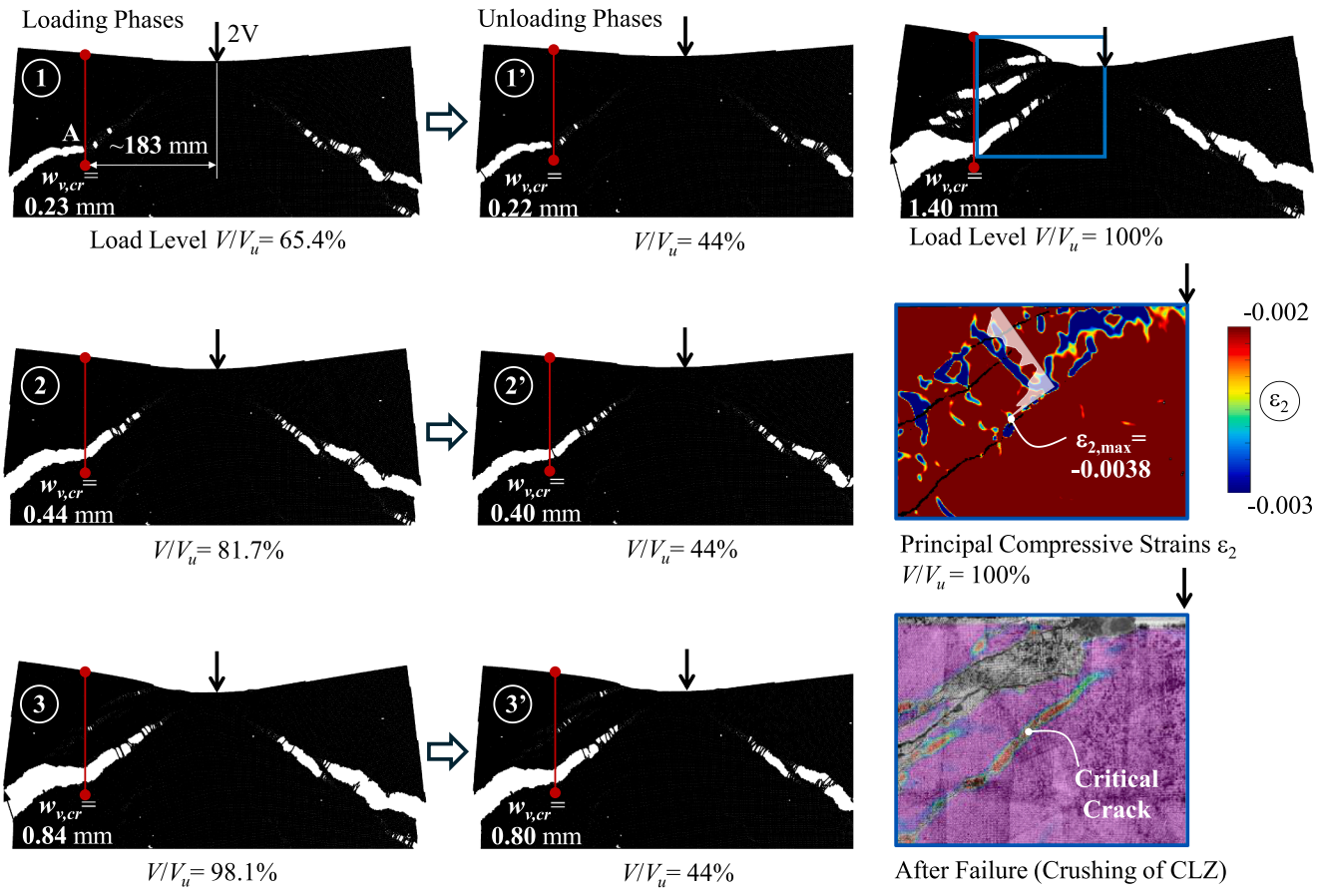

Fig. 6. Deformations in the critical loading zone of specimen P8 (on the left side of the load is the critical East shear span): a) deformed shapes, and b) failure pattern.

the flexural-tensile reinforcement $\varepsilon_{t,avg}$, which is associated with a flexural deformation pattern. The second DOF is the transverse displacement in the CLZ Δ_c, which is associated with a shear deformation pattern. The concrete block above the critical crack is modelled as rigid. The flexural DOF is associated with rotation of the block about point O and opening of the critical crack, while the shear degree of freedom represents a vertical translation of the block and an equivalent vertical displacement in the crack. The kinematics in Fig. 7a has been used to derive expressions for important deformations along the critical crack, including the crack width w, crack slip s, stirrup strain ε_v, and maximum compressive strain in the critical loading zone ε_{max}. All these deformations are expressed as functions of the two DOFs of the kinematic model (see [17] for complete expressions). Note also that w and s are calculated separately for each segment of the critical crack, and can vary significantly along the crack.

The local deformations and DOFs of the kinematic model are used to evaluate the shear-resisting mechanisms across the critical diagonal crack – see Fig. 7b. This is achieved by means of appropriate constitutive relationships. Four shear mechanisms are considered in the 2PKT: the shear carried in the CLZ V_{CLZ}, aggregate interlock shear V_{ci}, tension in the transverse web reinforcement (stirrups) V_s, and dowel action of the flexural reinforcement V_d. Shear component V_{CLZ} has been expressed with the compressive strain in the CLZ ε_{max}, V_{ci} with crack displacements w and s, V_s with the stirrup strain ε_v, and V_d with DOFs Δ_c and $\varepsilon_{t,avg}$ (see [17,20] for complete expressions). The measured geometry of the diagonal crack allows these mechanisms to be evaluated in a detailed crack-specific manner throughout the predicted response of the beam up to failure. In particular, the crack geometry has a significant impact on shear contributions V_{CLZ} and V_{ci} as demonstrated by Trandafir et al. [17,18]. In addition to the shear contributions, the 2PKT also uses a constitutive relationship to evaluate the tension in the flexural reinforcement T as a function of the strain in the reinforcement $\varepsilon_{t,avg}$ [17,20].

Finally, the 2PKT includes two equilibrium conditions – see Fig. 7c. They express the vertical equilibrium of the concrete block above the critical crack (left free body in Fig. 7b), as well as the moment equilibrium of the entire shear span (right free body in Fig. 7b). All forces in these equations are expressed with local deformations, and thus with the two DOFs of the 2PKT. Therefore, for a given shear force V, the two DOFs are obtained by solving the two equilibrium equations. The solution is iterative as the equations are nonlinear [17]. Calculations are performed for increasing values of V until the peak resistance (shear strength) V_u is reached.

3.2. Modelling of the CLZ

As the CLZ of deep beams crushes at failure, its modelling within the CBA approach [17,18] is discussed in more detail. This includes compatibility condition $\varepsilon_{max}=f(\Delta_c)$ and constitutive relationship $V_{CLZ}=f(\varepsilon_{max})$ indicated in Fig. 7.

In the original 2PKT [19], Mihaylov et al. (2013) have modelled the critical loading zone as shown in Fig. 8a based on experimental observations and stress analysis. The CLZ is idealized as a symmetrical triangle with angles α_{CLZ} representing the inclination of the critical crack in the vicinity of the loading plate. The length of the CLZ along the plate is denoted l_{b1e}. In the original 2PKT, angle α_{CLZ} and length l_{b1e} are predicted based on the properties of the beam. More specifically, α_{CLZ} is

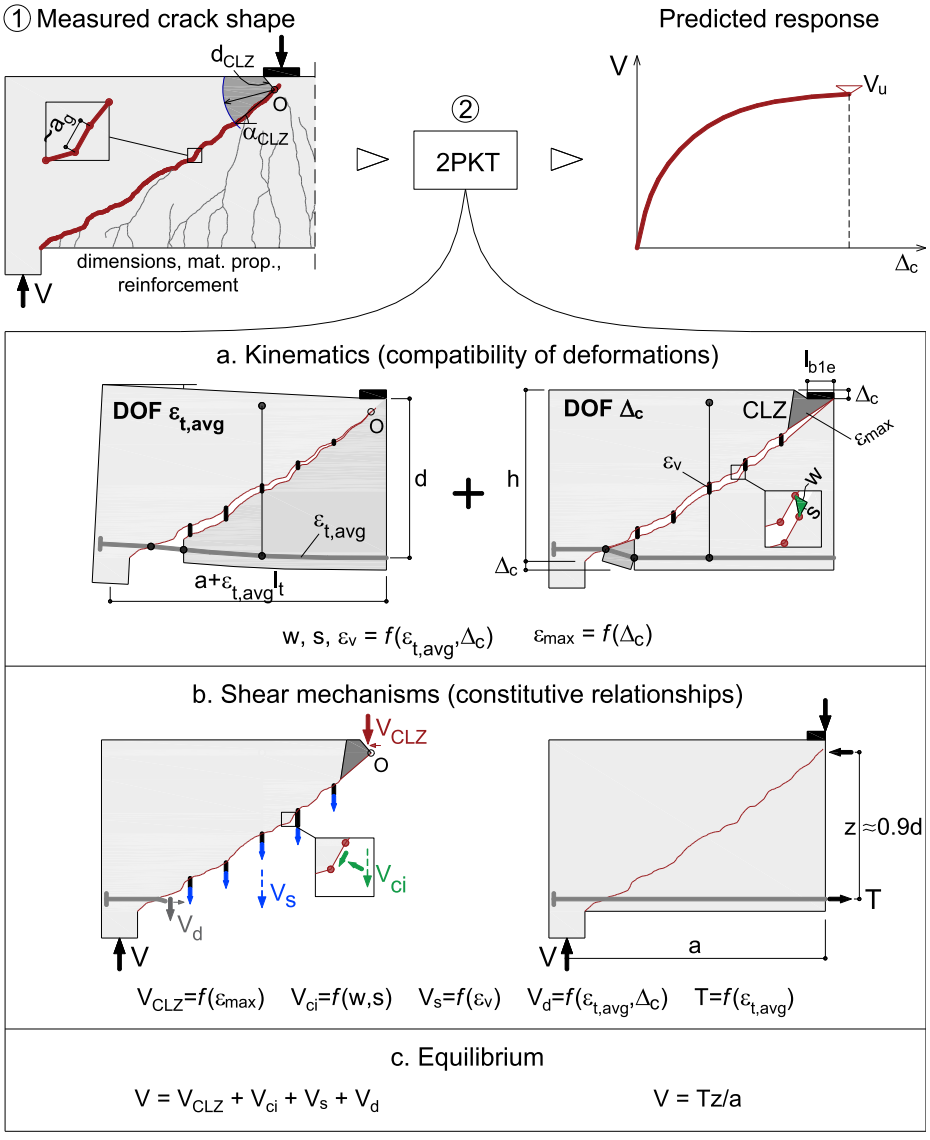

Fig. 7. Summary of crack-based assessment approach (CBA) [17,18] using the Two-Parameter Kinematic Theory (2PKT) [19,20].

estimated as the angle of the diagonal of the shear span, and l_{b1e} is the length along the loading plate responsible for the shear force V (e.g., one-half of the plate for symmetrical three-point bending). In terms of deformations, the compressive strain along the bottom face of the CLZ is ε_{max}, while the strain along the top face is assumed zero. The strains within the CLZ are assumed to vary linearly between zero and ε_{max}. These assumptions have been validated in several studies [18,19,24,25] and are consistent with the test results presented in Fig. 6. They lead directly to the following relationship between strain ε_{max} and DOF Δ_c (see [19]):

$$\varepsilon_{\max} = \frac{\Delta_c \tan\alpha_{CLZ}}{3l_{b1e}} \tag{1}$$

As with regards to relationship $V_{CLZ}=f(\varepsilon_{max})$, it is derived from the linear strain profile within the CLZ (Fig. 8a). The strains are transformed into stresses by using an appropriate constitutive relationship for concrete in uniaxial compression [26]. The stresses are integrated across the smallest section OB to obtain the resultant force in the CLZ inclined at angle α_{CLZ}. The vertical component of this force is the shear carried in the CLZ:

$$V_{CLZ} = \sigma_{avg}(\varepsilon_{\max}) b d_{CLZ} \sin\alpha_{CLZ}$$

$$\sigma_{avg} = \frac{\int_0^{\varepsilon_{\max}} \sigma_c(\varepsilon_c) d\varepsilon}{\varepsilon_{\max}} \tag{2}$$

where σ_{avg} is the average compressive stress in the CLZ, b is the width of the rectangular section of the beam, and d_{CLZ} is the depth of section OB equal to $l_{b1e}\sin(\alpha_{CLZ})$.

It is evident from Eqs. 1 and 2 that the predicted behavior of the CLZ is very much influenced by the estimated values of l_{b1e} and α_{CLZ}, or equivalently by the values of d_{CLZ} and α_{CLZ}. At the same time, these geometrical properties are very sensitive to random variations in the path of the critical diagonal crack in the vicinity of the loading plate. For this reason, in the crack-based assessment approach (CBA), d_{CLZ} and α_{CLZ} are obtained directly from the measured geometry of the crack. This is achieved as illustrated in Fig. 8b based on a procedure proposed by Trandafir et al. [17]. The following two steps are conducted to measure d_{CLZ} and α_{CLZ}:

1) Draw a line that connects the edge of the loading plate B to the closest point along the critical crack. The closest point is marked as point O in Fig. 8b. Line OB should be approximately perpendicular to the critical crack. The measured length of the line is d_{CLZ}.

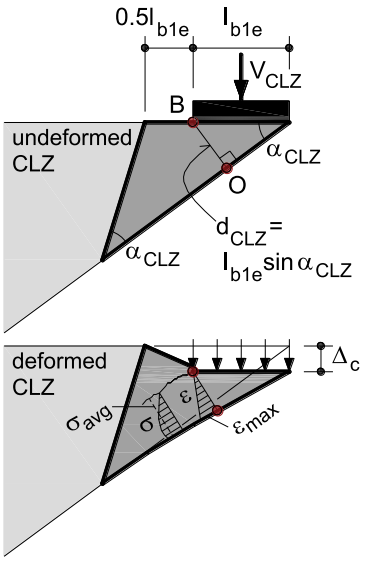

a) Model of critical loading zone [19]

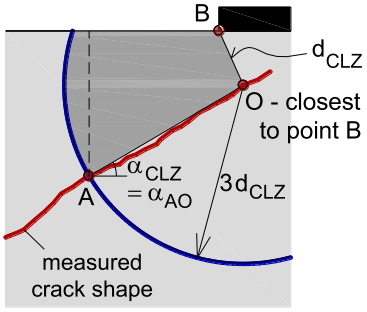

b) Method for measuring d_{CLZ} and α_{CLZ} [17]

Fig. 8. Crack-based modeling of the critical loading zone (CLZ).

2) Draw a circle with a center at point O and a radius of $3d_{CLZ}$. The circle intersects the critical crack at point A. Angle α_{CLZ} is measured as the angle of line AO with respect to the horizontal axis.

If the values of d_{CLZ} and α_{CLZ} differ substantially between the two faces of the beam, the average values can be used to generate the V_{CLZ}=f[$\varepsilon_{max}(\Delta_c)$] response. Radius $3d_{CLZ}$ and point A determine approximately the edge of the CLZ along the critical crack. Note that the theoretical radius based on Fig. 8a equals $2d_{CLZ}.\cot(\alpha_{CLZ})$, but is simplified to $3d_{CLZ}$ (i.e., $\cot\alpha_{CLZ}\approx1.5$) to allow for straightforward onsite measurements. Namely this simple two-step method was utilized in Fig. 6 to locate point A in the east shear span of specimen P8. Therefore, point A in Fig. 6 marks the estimated edge of the CLZ in the tested beam, as determined by the measured shape of the critical diagonal crack in the vicinity of the loading plate. Point A also defines the position of the critical vertical crack displacement $w_{v,cr}$.

3.3. Correspondence between DOF Δ_c of the 2PKT and the critical vertical crack displacement $w_{v,cr}$

As DOF Δ_c of the 2PKT characterizes the deformations in the CLZ, it is of interest to relate it to the crack measurements in Fig. 6. To this end, it is instructive to compare Fig. 6 to the idealized deformation patterns in Fig. 7a. This comparison shows that the shear degree of freedom Δ_c is nearly identical to the vertical crack displacement $w_{v,cr}$. This is because the flexural DOF of the kinematic model, $\varepsilon_{t,avg}$, has a negligible influence on the crack displacements in the vicinity of the load. Therefore, the crack-based 2PKT can be used to predict the measured crack displacement $w_{v,cr}$ as equal to Δ_c. To achieve a nearly complete correspondence between the predicted Δ_c and measured $w_{v,cr}$, it is necessary to measure $w_{v,cr}$ at the edge of the CLZ, i.e. at point A according to Fig. 8b. At this location Δ_c is fully developed, while the influence of $\varepsilon_{t,avg}$ is negligible. The measured $w_{v,cr}$ in Fig. 6 corresponds exactly to this location in specimen P8. For this specimen, d_{CLZ} and α_{CLZ} were measured respectively at 54 mm and 41° on the face of the DIC measurements. As a result, $w_{v,cr}$ is extracted from the DIC measurements at a horizontal distance of 183 mm from the center of the load (Fig. 6) The average values of d_{CLZ} and α_{CLZ} between the two faces of the beam are 43 mm and 38°. These average values are used for the crack-based 2PKT simulations presented next.

3.4. Predicted response of specimen P8

The main results from the CBA approach for the critical shear span of specimen P8 are shown in Fig. 9a. The plot compares the predicted and measured response in terms of shear force V versus the critical vertical crack displacement $w_{v,cr}\equiv\Delta_c$. The shear force is the sum of the four shear-resisting components V_{CLZ}, V_{ci}, V_s, and V_d predicted by the 2PKT, which are also shown in the plot. It can be seen that the measured response was nonlinear from the moment the critical crack formed at 225 kN up to the peak response (shear failure). It can also be seen that $w_{v,cr}$ does not recover upon unloading as already demonstrated with

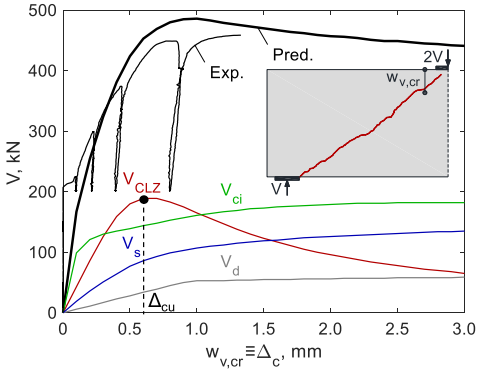

a) Measured and predicted critical crack displacement $w_{v,cr}$

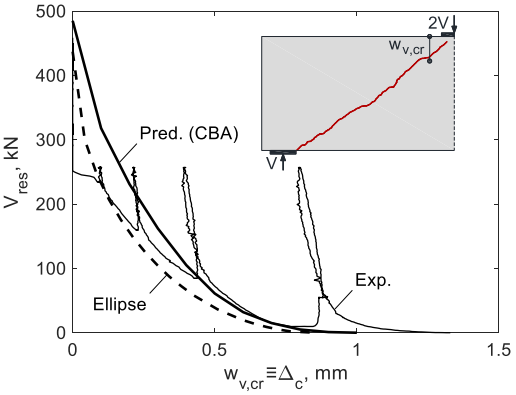

b) Residual shear strength with an elliptical approximation

Fig. 9. 2PKT analysis of specimen P8.

reference to Fig. 6. The measured unloading branches remain nearly vertical independently of the load level at which the unloading was initiated. Most importantly, a good agreement is achieved between the measured and predicted monotonic response in terms of envelope curves.

In terms of shear mechanisms, the aggregate interlock V_{ci} was activated rapidly at small values of $w_{v,cr}$, which explains the stiff initial response observed in the test. The second stiffest mechanism was the CLZ V_{CLZ}, followed by the stirrups V_s, and dowel action V_d. Near failure, the aggregate interlock and stirrups were in the plastic regime, thus producing a flat plastic plateau in terms of V-$w_{v,cr}$ response. It can be seen that the failure was triggered by the CLZ, whose resistance dropped quickly in the post-peak regime. As a result, the failure of the beam and the failure of the CLZ are almost coincident in terms of $w_{v,cr}$ values. This shows that, in order to predict $w_{v,cr}$ at the failure of the beam, it is only necessary to predict the displacement capacity of the CLZ, independently of the other shear mechanisms. This observation is fundamental for the development of the simplified crack-based assessment approach in the following section. The displacement capacity of the CLZ is denoted as Δ_{cu} in Fig. 9a.

Fig. 9b presents the same information but in a different format: on the horizontal axis is again $w_{v,cr}$=Δ_c, while on the vertical axis is the residual shear capacity V_{res}= (V_u-V). The dashed curve in this plot is neither experimental nor predicted by the CBA. It is an ellipse passed through points (Δ_c=0, V_{res}=V_u) and (Δ_c=Δ_{cu}, V_{res}=0). The center of the ellipse is placed at (Δ_c=Δ_{cu}, V_{res}=V_u). As a result, the ellipse has a vertical tangent at Δ_c= 0 and a horizontal tangent at Δ_c= Δ_{cu} (failure). These properties reflect very well the physics of the problem at hand, as the ellipse approximates well the initial stiff response and the final plastic plateau observed in the test and 2PKT predictions. It can be seen that the ellipse represents a nearly perfect fit to the complete measured V_{res}-$w_{v,cr}$ response of specimen P8 up to failure. Therefore, this elliptical shape, together with an appropriate prediction of Δ_{cu}, will be exploited further for the development of the simplified CBA.

4. Proposed novel simplified CBA for rapid assessment

4.1. Key observations from experiments and modelling

The experimental results from specimen P8 presented in Section 2, together with the crack-based 2PKT analysis results presented in Section 3, lead to several important observations. These observations are summarized below in order to establish the physical basis of the simplified crack-based assessment approach:

- The failure of deep beams is triggered by crushing of the critical loading zone (CLZ), whose geometry can be established by measuring two quantities: depth d_{CLZ} and angle α_{CLZ}.
- The deformations of the critical loading zone can be quantified by measuring the critical vertical crack displacement $w_{v,cr}$ at the edge of the CLZ.
- At the failure of the beam, the critical crack displacement $w_{v,cr}$ reaches the displacement capacity of the CLZ Δ_{cu}.
- The V-$w_{v,cr}$ response is initially very stiff due to aggregate interlock and becomes very flat at failure when the shear-resisting mechanisms enter the plastic regime.
- The critical crack displacement $w_{v,cr}$ does not recover upon unloading at any load level.

These observations, while illustrated here with the help of specimen P8, are consistent with abundant experimental data and modelling results presented in various previous studies by the authors and others [17–20,24,25,27–30]. In the following, they are used to build the simplified CBA approach.

4.2. Formulation of the simplified CBA

Based on these observations, a five-step procedure for rapid crack-based assessment of cracked deep beams is proposed. The five steps are listed and justified in the following:

1) Inspect the CLZ of the beam for the presence of inclined macrocracks. If such cracks have occurred, the member is in distress and urgent measures are needed to avoid failure.
2) If inclined cracks are not present, proceed to measure the geometry of the critical loading zone – i.e. distance d_{CLZ} and angle α_{CLZ} – as described with regards to Fig. 8b (see two-step procedure in Section 3.2).
3) Calculate the displacement capacity of the CLZ, Δ_{cu} as:

$$\Delta_{cu} = 0.009 d_{CLZ} \frac{\cos\alpha_{CLZ}}{\sin^2\alpha_{CLZ}} \tag{3}$$

4) Measure the critical vertical crack displacement $w_{v,cr}$ at the edge of the CLZ, i.e. at point A in Fig. 8b.
5) Calculate the residual capacity of the beam ψ for the measured critical crack displacement $w_{v,cr}$ using Eq. 4. The residual capacity is expressed as a percentage of the shear strength:

$$\psi(w_{v,cr}) = \left(1 - \frac{V}{V_u}\right) \times 100 = 0.9\left[1 - \sqrt{1 - \left(1 - \frac{w_{v,cr}}{\Delta_{cu}}\right)^2}\right] \times 100, \% \tag{4}$$

The first step in this procedure is justified by the nature of the macrocracks in the CLZ. They occur when the CLZ is crushing and the beam is on the verge of failure. In specimen P8, the macrocracks developed at 97% of the failure load. No further assessment can be justified at this stage and urgent safety measures are required.

Eq. 3 is derived directly from Eq. 1, which was itself derived earlier from the model of the CLZ in Fig. 8a. It assumes that the compressive strain along the bottom face of the CLZ ε_{max} reaches 3×10^{-3} at failure, which is consistent with DIC measurements and observed concrete crushing. It also takes into account that l_{b1e} is equal to $d_{CLZ}/\sin(\alpha_{CLZ})$.

Eq. 4 uses a simple approximation of the shape of the V_{res}-$w_{v,cr}$ response. Taking into account the stiff initial response and flat ultimate response, the V_{res}-$w_{v,cr}$ curve is approximated with an ellipse as shown earlier in Fig. 9b. The ellipse has a vertical tangent at $w_{v,cr}$= 0 and a horizontal tangent at $w_{v,cr}$= Δ_{cu}. The peak resistance V_u, and therefore zero residual capacity ψ, is reached when $w_{v,cr}$ reaches the displacement capacity of the CLZ Δ_{cu} obtained from Eq. 3. The factor of 0.9 in Eq. 4 is applied to the ellipse to introduce a certain conservatism in the estimated residual capacity.

It is important to emphasize the meaning of the residual capacity $\psi(w_{v,cr})$ in the presence of earlier loading and unloading cycles. Because $w_{v,cr}$ does not recover upon unloading, $\psi(w_{v,cr})$ does not necessarily signify the residual capacity under the current load on the structure. Instead, it shows the closest the structure has come to failure during its entire service life up to the moment of measuring $w_{v,cr}$. In other words, the proposed novel approach allows to access a "memory" the structure keeps of the largest load it has experienced during its entire loading history. This information can be of significant practical importance, as it speaks not only of the structure itself, but also of the long-term loading history experienced by the structure.

4.3. Validation of the simplified CBA

The rapid crack-based assessment approach presented in Section 4.2 is validated with several tests from this and previous studies [25,27–29]. The properties of the test specimens are summarized in Table 1. The effective depth of the beams d varies from 732 mm to 3840 mm, the a/d

Table 1
Summary of beam properties.

Beam	a/d -	d mm	ρ_l %	ρ_v %	f_c MPa	d_{CLZ} mm	α_{CLZ} deg	$\Delta_{cu,pred}$ mm	$\Delta_{cu,exp.}$ mm	$V_{u,exp}$ kN
P8	1.64	732	1.37	0.134	39.7	54	41	0.85	1.40	459
P3	1.64	732	1.37	0.134	40.5	74	34	1.77	1.60	466
CCR2	2.00	1105	2.10	0.141	35.8	127	30	3.83	3.38	1118
PLS4000W	1.82	3840	0.66	0.080	44.2	123	32	3.29	3.47	1509
S1M	1.55	1095	0.70	0.101	33.0	59	36	1.25	-	941
S0M	1.55	1095	0.70	0	34.2	34	30	1.01	-	721

a= shear span; d= effective depth; ρ_l= flexural reinforcement ratio; ρ_v= transverse reinforcement ratio; f_c= concrete compressive strength; d_{CLZ}= measured depth of critical loading zone, α_{CLZ}= measured angle of critical crack in critical loading zone; $\Delta_{cu,pred.}$= predicted displacement capacity of the CLZ using Eq. 3; $\Delta_{cu,pred.}$= measured displacement capacity of the CLZ ($w_{v,cr}$ at beam failure); $V_{u,exp.}$= measured shear strength.

ratio from 1.55 to 2.00, the flexural reinforcement ratio ρ_l from 0.66% to 1.37%, the transverse reinforcement ratio ρ_v from 0 to 0.141%, and the concrete compressive strength f_c varies from 33.0 MPa to 44.2 MPa. Only tests that included measurements of the critical crack displacements $w_{v,cr}$ are selected for this study in order to be able to perform validations. Detailed crack photos/diagrams were also necessary in order to measure the geometry of the critical loading zones as described in Fig. 8b. No other restrictive criteria were used in the selection of test specimens.

Fig. 10 shows the predicted residual capacity diagrams of specimens P8 and P3 obtained from Eqs. 1–2 (P3 was reported earlier by Fathalla and Mihaylov [25]). They are compared with the experimental residual capacity curves, where $w_{v,cr}$ is measured at the edge of the CLZ (point A in Fig. 8b). The two specimens were nominally identical, except for the compressive strength of the concrete which differed very slightly (39.7 MPa for P8 vs. 40.5 MPa for P3). Nevertheless, the two measured ψ curves are significantly different. The reason for this difference is different d_{CLZ} and α_{CLZ} due to random variations in the path of the critical cracks in the vicinity of the loading plate. The measured geometry of the CLZ and the corresponding predicted values of Δ_{cu} are reported in Table 1. Specimen P3 had a deeper CLZ and a flatter critical crack, both of which result in a larger displacement capacity Δ_{cu} according to Eq. 3. The figure shows the adequacy of Eqs. 3 and 4 when compared to the experimental results for the complete range of crack displacements from zero to Δ_{cu}. It is seen that the simplified CBA predicts well the residual shear capacity of both specimens using minimum input information and only two simple equations.

The comparisons in Fig. 10 focused on the critical shear spans of specimens P3 and P8. However, in a realistic crack-based assessment of existing deep beams, the critical shear span is not known in advance, and the assessment needs to be performed on both sides of the loading plate/element. Therefore, it is of interest to verify whether the proposed parsimonious crack-based assessment approach can accurately predict the critical shear span solely using Eq. 3 and Eq. 4.

This is illustrated in Fig. 11 for specimen P8. On the horizontal axis of the plot is the normalized point load P/P_u at which the assessment is performed, and on the vertical axis is the predicted residual capacity ψ from Eqs. 3–4. The predictions are made separately for the east and west shear spans using the respective measured values of d_{CLZ}, α_{CLZ} and $w_{v,cr}$. The values of d_{CLZ} and α_{CLZ} are shown on the crack diagram of the beam in the vicinity of the applied load (Fig. 11 top). The assessment is conducted at four load levels P/P_u: 49%, 65%, 82%, 89%, and 100%. The first level corresponds to the full propagation of the critical diagonal cracks, while the other levels correspond to the peaks of the load cycles up to failure (see Figs. 4 and 6). It can be seen that the assessment of the cracks on both sides of the load renders significantly different results. For the same load, the west crack measured consistently larger crack displacements $w_{v,cr}$ than the east crack. Nevertheless, the west shear span is predicted to have a larger residual capacity at all load levels. At 100% of the failure load, the proposed approach correctly predicts that the residual capacity of the critical east shear span is nearly zero. At the same time, the predicted residual capacity of the non-critical west crack

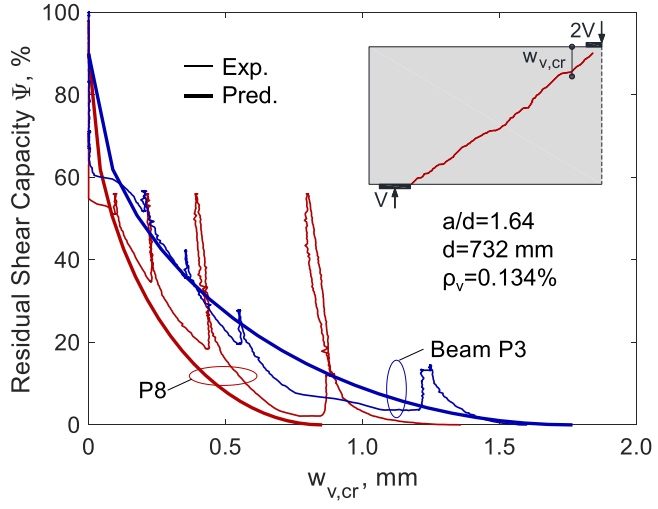

Fig. 10. Measured and predicted residual capacity diagrams of nominally identical specimens P8 (red) and P3 [25] (blue).

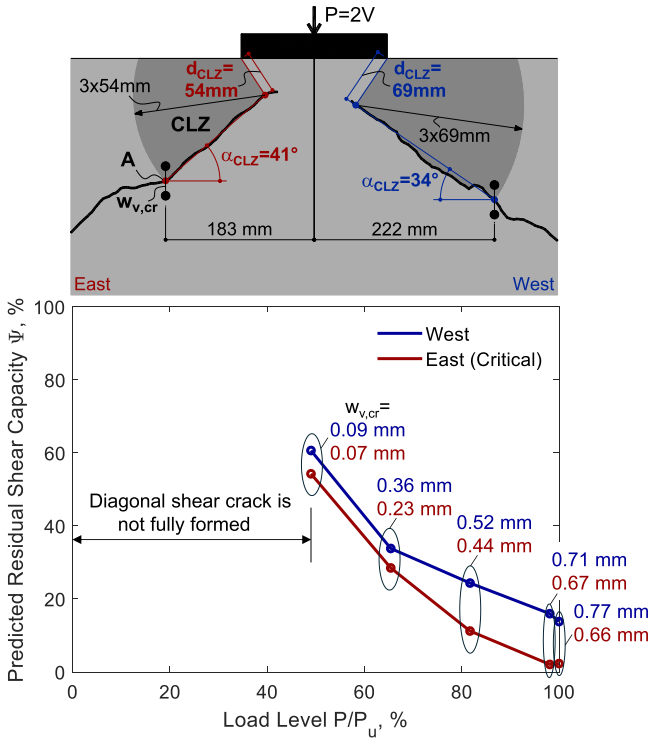

Fig. 11. Simultaneous crack-based assessment of the two shear spans of specimen P8.

is 13.8%. This demonstrates that the proposed crack-based assessment approach correctly predicts the critical shear span based solely on three measurements: d_{CLZ}, α_{CLZ}, and $w_{v,cr}$.

Fig. 12 shows validations of the proposed approach with the remaining tests from Table 1. Eqs. 3 and 4 show excellent predictions of residual capacity from zero critical crack displacement to failure. It is important to highlight that this conclusion is valid for specimens with very different properties, including a beam without shear reinforcement (specimen S0M) and a 4m-deep beam (PLS4000W). As listed in Table 1, the predicted displacement capacities of the CLZ Δ_{cu} vary from 0.85 mm to 3.8 mm, and agree reasonably well with the measured values provided in the same table.

4.4. Limits of applicability and uncertainties

Despite the broad range of test variables considered in the validations in Figs. 10–12, the simplified crack-based approach has several limits of applicability. It is developed for shear spans of deep beams, and therefore the shear-span-to-effective-depth ratio a/d ratio is limited to a maximum of 2. The method can be used if the diagonal crack is fully developed from the support to the near vicinity of the load (or vice versa). This ensures that no new major shear cracks can propagate to the vicinity of the load, and thus alter the geometry and displacement capacity of the CLZ. It also ensures that d_{CLZ} can be measured as the depth of the section which is approximately perpendicular to the critical crack (Fig. 8b). In addition, shear spans subjected to double curvature are also outside the scope of this study. Such cases arise in continuous deep beams, where additional cracks can form in the CLZ due to tension in the reinforcement crossing this zone [31]. Furthermore, it is imperative to ensure that the flexural-tensile reinforcement is sufficient to prevent flexural failure and is well anchored in the support zones. If the reinforcement is not well anchored, that will lead to additional opening of the critical diagonal crack, and thus larger $w_{v,cr}$. This unfavorable effect is indirectly captured by the proposed crack-based assessment method, as the predicted residual capacity $\psi(w_{v,cr})$ will decrease. The presence of compression flanges also limits the applicability of the method, as they modify the geometry and behavior of the CLZ. Finally, in terms of reinforcement, the crack-based approach is of most interest for assessment of existing members with less-than-minimum transverse reinforcement according to modern standards (approx. $\rho_v \leq 0.20\%$). Such members develop a dominant diagonal crack and are outside the range of applicability of conventional plasticity approaches for strength evaluation (i.e., strut-and-tie and stress field models).

One of the main uncertainties in the application of the proposed method arises from the large variety of loading and support elements encountered in existing structures. For example, pier cap beams in bridges are often loaded by beam bearings that are significantly narrower than the width of the beam, and/or are supported by circular piers. Both these cases create uncertainties with regards to the geometry of the CLZ and the crack measurements in the vicinity of the bearing/

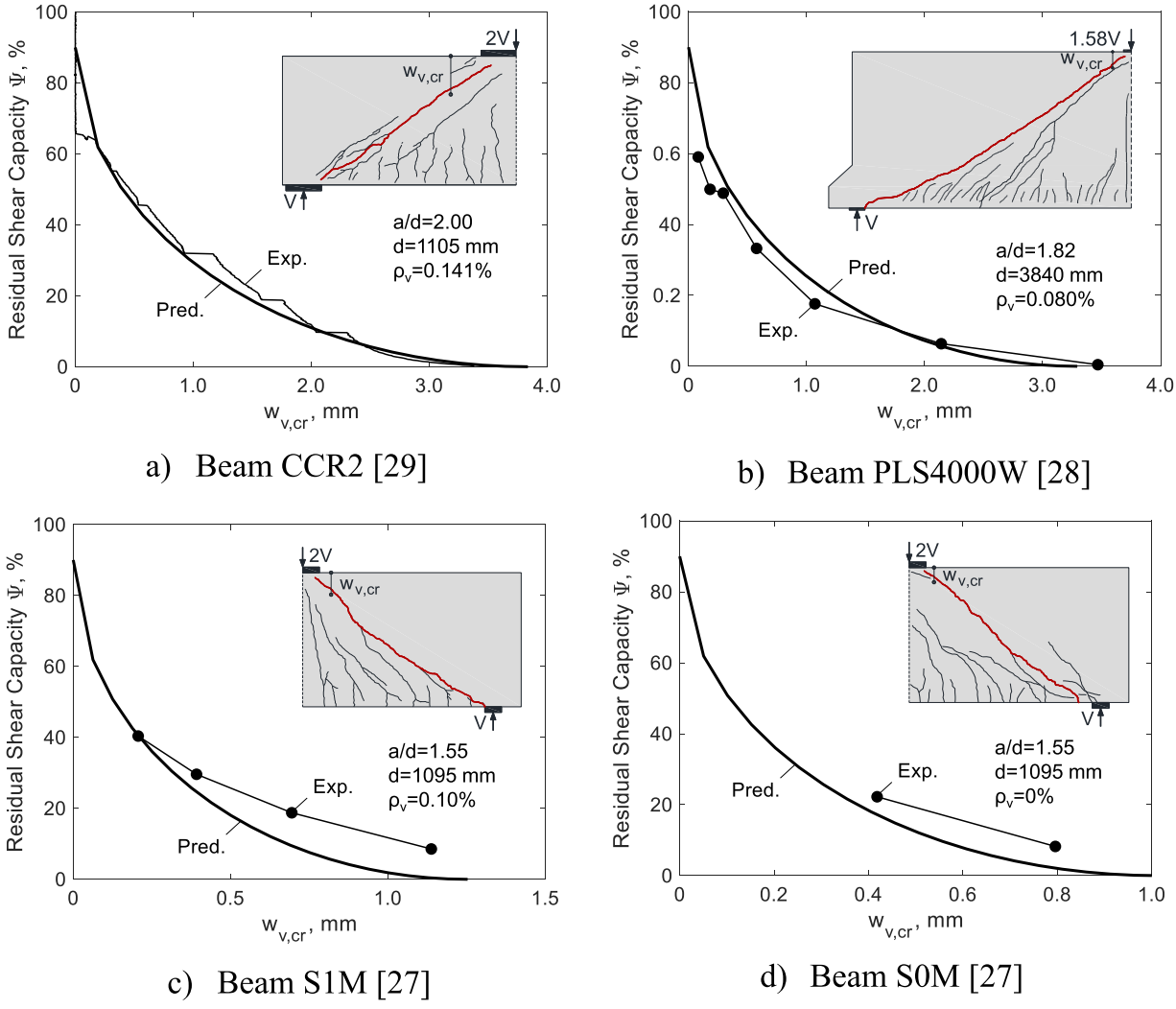

Fig. 12. Measured and predicted residual shear capacity diagrams of specimens with variable properties.

column. Other sources of uncertainty that require further investigation include tapered members, eroded crack faces, presence of corrosion, creep and fatigue. Some of these factors are discussed further in the following.

5. Discussion

The proposed crack-based assessment approach (CBA) has some important implications and opens new promising perspectives, which are discussed in the following.

5.1. Minimal required information for assessment

As has already been demonstrated, the proposed CBA (Section 4.2) requires minimal input information and computational effort to produce accurate results. The input consists of only three measurable quantities (d_{CLZ}, α_{CLZ}, and $w_{v,cr}$) that are used in conjunction with two simple closed-form equations (Eqs. 3 and 4). At the same time, it is important to highlight the information which is not used/required by the method. This includes the size of the member, the a/d ratio, the amount of shear reinforcement, the concrete strength, and all other properties of the beam. It was illustrated that these properties are not decisive when evaluating the residual shear capacity as a fraction of the peak resistance, even though they are very important when calculating the absolute resistance (in kN). This makes the proposed method very convenient as often in existing structures detailed information on reinforcement and material properties are not readily available. In such cases, a series of surveys and non-destructive tests need to be conducted before performing detailed assessment calculations (e.g., core sampling, reinforcement mapping, etc.). In addition, the proposed assessment method captures the effect of random variations in the paths of the critical cracks (Figs. 10 and 11), which impact the size and shape of the CLZ. These effects are not captured by other modelling techniques, including complex numerical models.

5.2. Absolute residual shear capacity and levels of approximation (LoA)

All of the above concerned the assessment of the residual shear capacity of deep beams as a percentage of the shear capacity. However, it is also of interest to assess the residual capacity in terms of absolute shear force V_{res}. Here again the proposed assessment approach can be very useful. To evaluate the residual capacity curve $V_{res}(w_{v,cr})$, it is only necessary to multiply the $\psi(w_{v,cr})$ diagram given by Eq. 3 with the predicted shear strength of the member V_u. The shear strength can be evaluated with any appropriate method available to the engineer, including strut-and-tie models, the original 2PKT method, stress field models or even nonlinear finite element models. In this way, the engineer can establish levels of approximation (LoA) as illustrated in Fig. 13. A simple approach, such as a strut-and-tie model, can provide the lowest level of approximation (LoA I) that requires limited computational effort but renders a conservative assessment. If this LoA shows that the residual shear capacity is insufficient, or if the lowest LoA is not applicable (e.g., strut-and-tie models may not be applicable to members with less-than-minimum transverse reinforcement), the engineer can proceed to a higher level of approximation for enhanced V_u predictions. If the negative consequences of closing the structure are deemed very important, a third and highest level of approximation LoA III can be employed to minimize the conservativeness of the structural assessment (e.g., detailed stress field analysis).

5.3. Creep and fatigue effects

This study does not address the long-term effects of creep and fatigue, which are inevitably present in concrete infrastructure. Both these effects will result in increasing critical crack displacement $w_{v,cr}$ over time [25,32]. Further studies are needed to study creep and fatigue in the context of crack-based assessment. Nevertheless, even in its current form, the proposed assessment method produces adequate trends. As long-term effects progress and $w_{v,cr}$ increases, Eqs. 3 and 4 will predict that the residual capacity decreases, which is consistent with the influence of creep and fatigue on the shear strength. Furthermore, this applies to any unfavorable effect that may result in additional opening of the critical crack. As mentioned earlier, additional opening can also arise from inadequate anchorage of the flexural reinforcement in the support zones. In this case again the proposed method will signal that the residual capacity is decreasing.

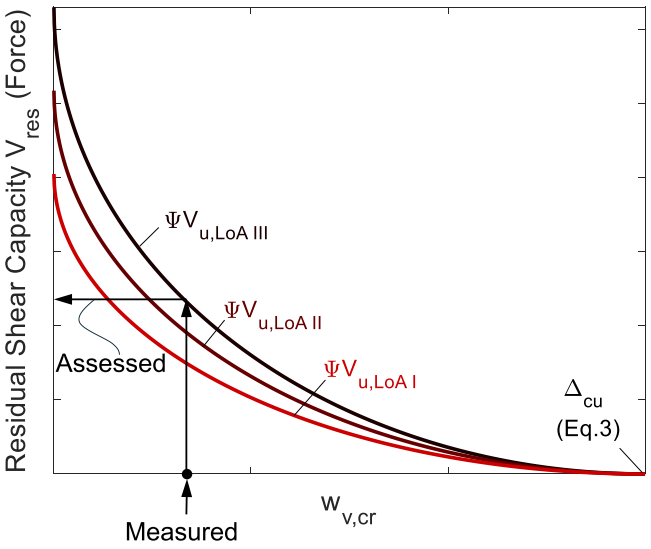

Fig. 13. Absolute residual shear capacity of deep beams based on a selected LoA.

5.4. Monitoring of shear-critical deep beams in concrete infrastructure

The method presented in Section 4.2 is not only suitable for a single-time assessment, but can also be employed for long-term monitoring of deep beams with diagonal cracks. To this end, an initial assessment needs to be performed as described before to measure the geometry of the CLZ and the current critical crack displacement $w_{v,cr0}$. Following this stage, it is recommended to install a vertical displacement transducer to measure the increment of the crack displacement, $\Delta w_{v,cr}$, over time. The transducer must be connected immediately below the critical crack and at the top edge of the beam as shown in Fig. 6. In this way, the sum of the initial measurement $w_{v,cr0}$ and the reading of the transducer $\Delta w_{v,cr}$ provides the complete transverse deformation of the CLZ $w_{v,cr}$, including cracking in the CLZ. This is of key importance, as inclined diagonal cracks may form in the CLZ near failure, and they need to be captured by the transducer. Because $w_{v,cr}$ does not recover upon unloading, the monitored values can only increase over time due to large variable loads or long-term effects. As illustrated in Fig. 14, the monitored values of $w_{v,cr}$ can then be used in conjunction with Eqs. 3 and 4 to continuously monitor the residual capacity of the member. The plot demonstrates how convenient the critical vertical crack displacement $w_{v,cr}$ is for monitoring. Regardless of the loading history, $w_{v,cr}$ only increases over time, and therefore the residual capacity decreases monotonically until it reaches an imposed threshold linked to safety or planned intervention/maintenance.

6. Conclusions

This paper presented a rational approach for rapid assessment of the residual capacity of deep beams with diagonal cracks. The residual capacity is evaluated for a measured vertical crack displacement at the

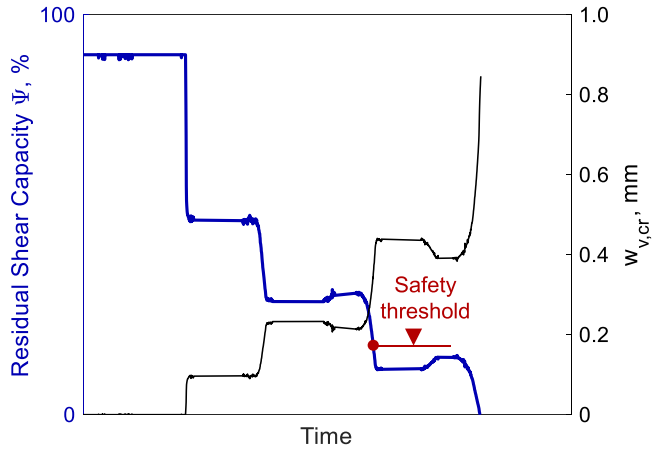

Fig. 14. Concept of structural monitoring of deep beams with diagonal cracks (based on data from specimen P8).

edge of the critical loading zone (CLZ). The physical basis of this crack-based assessment approach (CBA) was established with the help of a targeted test and advanced crack-based analysis. The CBA was validated with measured residual capacity diagrams, showing accurate results. The main conclusions of the study are the following:

1) The shear failure of deep beams is triggered by crushing of the concrete in the CLZ. Therefore, crack-based assessment approaches should focus on evaluating the state of damage of the CLZ.
2) The proposed approach uses only three measurements in the CLZ, together with two simple closed-form equations, to accurately evaluate the residual shear capacity of the member as a percentage of the shear strength. The measurements include the depth of the CLZ determined by the critical diagonal crack, the angle of the crack in the CLZ, and the critical vertical displacement in the crack at the edge of the CLZ. No additional input information is required for the assessment (e.g., members size, a/d ratio, reinforcement and material properties). Therefore, this is an approach that combines parsimony with high accuracy and explaining power.
3) The critical vertical crack displacement does not recover upon unloading. Therefore, the evaluated residual capacity shows what is the closest the cracked deep beam has come to failure during its entire service life up to the moment of assessment. In this manner, the proposed CBA reveals important "memory" of the history of loading and safety of the member.
4) The proposed CBA is also well suited for long-term monitoring of the residual capacity of cracked deep beams. The monitoring can be performed in an automated manner by imposing appropriate thresholds on the residual capacity, which decreases monotonically over time.

Further research is required to study sources of uncertainty in practical applications, such as different geometries of loading and support elements (e.g., small bearings, circular columns), tapered members, creep and fatigue effects.

CRediT authorship contribution statement

Boyan Mihaylov: Writing – original draft, Validation, Supervision, Project administration, Methodology, Investigation, Funding acquisition, Conceptualization. **Eissa Fathalla:** Writing – review & editing, Visualization, Validation, Software, Investigation. **Alexandru Trandafir:** Writing – review & editing, Visualization, Validation, Software, Investigation.

Declaration of Competing Interest

The authors declare that they have no known competing financial interests or personal relationships that could have appeared to influence the work reported in this paper.

Data availability

Data will be made available on request.

References

[1] Bracci JM, Keating PB, Hueste MBD. Cracking in RC Bent Caps. Report No. 1851-1. The Texas A&M University; 2000.
[2] Aravinthan T, Suntharavadivel TG. Effects of existing shear damage on externally posttensioned repair of bent caps. J Struc Eng 2007;133(11):1662–9.
[3] Birrcher D, Tuchscherer R, Huizinga M, Bayrak O, Wood SL, Jirsa JO. Strength and serviceability design of reinforced concrete deep beams. Report No. FHWA/TX-09/0-5253-1. The University of Texas at Austin,; 2009.
[4] Larson N, Gomez EF, Garber D, Bayrak O, Ghannoum WM. Strength and Serviceability Design of Reinforced Concrete Inverted-T Beams. Report No. FHWA/TX-13/0-6416-1. The University of Texas at Austin; 2013.
[5] Clark AP. Diagonal tension in reinforced concrete beams. Acids Struct J 1951;48(10):145–56.
[6] Leonhardt F, Walther R. "The Stuttgart Shear Tests 1961" – A translation of the articles that appeared in Beton und Stahlbetonbau, 56(12) in 1961 and 57(2,3,6- 8) in 1962. Cement and Concrete Association Library Translation No. 111. UK: Wexham Springs,; 1964. p. 134.
[7] Rogowsky DM, MacGregor JG. Tests of reinforced concrete deep beams. Acids J Proc 1986;83(4):614–23.
[8] Schlaich J, Schäfer K, Jennewein M. Toward a consistent design of structural concrete. PCI J 1987;32(3):74–150.
[9] Collins MP, Mitchell D. Rational approach to shear design – the 1984 Canadian code provisions. Acids Struct J 1986;83(6):925–33.
[10] Muttoni A, Schwartz J, Thürlimann B. Design of concrete structures with stress fields. Basel, Switzerland: Birkhäuser Verlag,; 1996. p. 143.
[11] Campana S, Fernández-Ruiz M, Anastasi A, Muttoni A. Analysis of shear-transfer actions on one-way RC members based on measured cracking pattern and failure kinematics. Mag Concr Res 2013;65:386–404.
[12] Huber P, Huber T, Kollegger J. Investigation of the shear behavior of RC beams on the basis of measured crack kinematics. Eng Struct 2016;113:41–58.
[13] Fathalla E, Mihaylov B. Comprehensive approach for examining shear-critical RC walls using detailed experimental measurements. Struct Conc 2024. https://doi.org/10.1002/suco.202400276.
[14] Palipana DK, Trandafir AN, Mihaylov BI, Proestos GT. Quantification of shear transfer mechanisms in reinforced concrete deep beams using measured experimental data. Eng Struct 2024;318:118711.
[15] Li G, Liu Q, Zhao S, Qiao W, Ren X. Automatic crack recognition for concrete bridges using a fully convolutional neural network and naive Bayes data fusion based on a visual detection system. Meas Sci Technol 2020;31(7):075403.
[16] Pantoja-Rosero BG, dos Santos KM, Achanta R, Rezaie A, Beyer K. Determining crack kinematics from imaged crack patterns. Constr Build Mater 2022;343:128054.
[17] Trandafir AN, Palipana DK, Proestos GT, Mihaylov BI. Framework for Crack-Based Assessment of Existing Lightly-Reinforced Concrete Deep Members. Acids Struct J 2022;119(1):255–66.
[18] Trandafir AN, Proestos GT, Mihaylov BI. Detailed crack-based assessment of a 4-m deep beam test specimen. Struct Conc 2023;24(1):756–70.
[19] Mihaylov BI, Bentz EC, Collins MP. Two-parameter kinematic theory for shear behavior of deep beams. Acids Struct J 2013;110(3):447–55.
[20] Mihaylov B. Five-spring model for complete shear behaviour of deep beams. Struct Conc 2015;16(1):71–83.
[21] Calvi PM, Bentz EC, Collins MP. Model for assessment of cracked reinforced concrete membrane elements subjected to shear and axial loads. Acids Struct J 2018;115(2):501–9.
[22] Zaborac J, Athanasiou A, Salamone S, Bayrak O, Hrynyk TD. Crack-based shear strength assessment of reinforced concrete members using a fixed-crack continuum modeling approach. J Struc Eng 2020;146(4):04020024.
[23] Vecchio FJ, Collins MP. The modified compression-field theory for reinforced concrete elements subjected to shear. Acids Struct J 1986;83(2):219–31.
[24] Palipana DK, Trandafir AN, Mihaylov BI, Proestos GT. Framework for quantification of shear-transfer mechanisms from deep beam experiments. Acids Struct J 2022 May 1;119(3).
[25] Fathalla E, Mihaylov B. Fatigue behavior of deep concrete beams with critical shear cracks. Struct Conc 2023;24(6):7314–33.
[26] Popovics S. A numerical approach to the complete stress-strain curve of concrete. Cem Conc Res 1973;3(5):583–99.
[27] Mihaylov BI, Bentz EC, Collins MP. Behavior of large deep beams subjected to monotonic and reversed cyclic shear. Acids Struct J 2010;107(6):726–34.
[28] Collins M.P., Bentz E.C., Quach P.T. Shear Behavior of Thick Slabs. ACI Struct J, 117(4):115–126.

[29] Palipana DK, Proestos GT. Behavior of shear-critical concrete deep beams monitored with digital image correlation equipment. Acids Struct J 2024 Mar 1; 121(2).
[30] Proestos GT, Palipana DK, Mihaylov BI. Evaluating the shear resistance of deep beams loaded or supported by wide elements. Eng Struct 2021 Jan 1;226:111368.
[31] Mihaylov BI, Hunt B, Bentz EC, Collins MP. Three-parameter kinematic theory for shear behavior of continuous deep beams. Acids Struct J 2015;112(1):47–57.
[32] Mazzotti C, Savoia M. Nonlinear creep damage model for concrete under uniaxial compression. J Eng Mech 2003;129(9):1065–75.